

Article

Experimental Study for Understanding the Characteristics of a Floating Axis Wind Turbine under Wind and Wave Conditions

Hidetaka Senga ^{1,*}, Keitaro Kunishi ¹, Gaku Fujita ², Tomotake Imaoka ², Hiroyuki Ohira ² and Hiromichi Akimoto ³

¹ Department of Naval Architecture and Ocean Engineering, Graduate School of Engineering, Osaka University, Suita 565-0871, Osaka, Japan

² Electric Power Development Co., Ltd., 1-9-88, Chigasaki, Chigasaki 253-0041, Kanagawa, Japan

³ Albatross Technology Inc., 2-12-5, Nihonbashiningyocho, Chuo-ku, Tokyo 103-0013, Japan; akimoto@albatross-technology.com

* Correspondence: senga@naoe.eng.osaka-u.ac.jp; Tel.: +81-668-797-574

Abstract: Floating offshore wind turbines (FOWTs) are suitable for Japan's coastal waters. As one of the unique concepts of FOWTs, the floating axis wind turbine (FAWT) is a type of vertical axis wind turbine (VAWT) that actively uses the features of VAWTs to specialize in an area of the floating type. In this study, FAWT behaviors under wind and wave conditions were experimentally investigated in a water tank to understand its dynamic characteristics. The experimental results reveal that although the floater of the FAWT is relatively small compared to its rotor size, its heave response is comparable to those of the other FOWTs using different floaters. Moreover, the FAWT shows a high stability under rated operation and during sudden changes in the wind.

Keywords: floating axis wind turbine; model experiment; mooring



Citation: Senga, H.; Kunishi, K.; Fujita, G.; Imaoka, T.; Ohira, H.; Akimoto, H. Experimental Study for Understanding the Characteristics of a Floating Axis Wind Turbine under Wind and Wave Conditions. *Energies* **2024**, *17*, 3285. <https://doi.org/10.3390/en17133285>

Academic Editor: Francesco Castellani

Received: 6 June 2024

Revised: 2 July 2024

Accepted: 2 July 2024

Published: 4 July 2024



Copyright: © 2024 by the authors. Licensee MDPI, Basel, Switzerland. This article is an open access article distributed under the terms and conditions of the Creative Commons Attribution (CC BY) license (<https://creativecommons.org/licenses/by/4.0/>).

1. Introduction

In the field of renewable energies, floating offshore wind turbines (FOWTs) comprise one of the key technologies with high future growth potential in the renewable energy sector. We have several options to design a FOWT system, such as the types of wind turbines and floaters.

As for FOWTs with the horizontal axis wind turbine (HAWT), Takata et al. [1] focused on the elastic behavior of a FOWT associated with its cost reduction. Upon designing a flexible multi-column FOWT and conducting several water tank experiments, they found that dynamic elastic deformation affected the behavior of the FOWT. Another study designed a spar-type FOWT with a flexible backbone to reproduce an appropriate flexibility of the structure and observed a highly nonlinear hydro-elastic response [2]. A semisubmersible variant was also investigated for different shapes [3,4].

Meanwhile, FOWTs with the vertical axis wind turbine (VAWT) have also been experimentally and numerically investigated in the literature. For example, Ghigo et al. [5] reviewed various concepts. Among these, the DeepWind concept, one of the popular types of floating offshore vertical axis wind turbines [6], utilizes a Darrieus-type rotor and a slender cylindrical structure that rotates along with the rotor as its floating platform. In this system, the generator is located at the bottom of the cylindrical structure. Paulsen et al. [7] reported a 5 MW design optimization. Borg et al. [8] proposed a semisubmersible and tension-leg platform (TLP) type as the floating platform for the baseline 5 MW DeepWind VAWT rotor aside from the spar type and emphasized the importance of the mooring design. Ishie et al. [9] numerically analyzed a 5 MW optimized floating vertical axis wind turbine (FVAWT), which combines the optimized 5 MW DeepWind rotor from the Technical University of Denmark and the DeepCwind semisubmersible platform [10]. A 1 kW DeepWind demonstrator was experimentally investigated in the wind tunnel under the upright and tilted rotor conditions [11]. Meanwhile, Iwamatsu et al. [12] investigated the elastic

response of a FVAWT with two Darrieus-type rotors installed on the semisubmersible platform. The experimental results indicated that the thrust from the rotor increased the bending moment on the hull up to approximately 20%.

Hand et al. [13] numerically investigated a 5 MW floating VAWT with straight blades and concluded that the turbine solidity with 0.263 yielded the highest aerodynamic efficiency under their conceptual design. The tip vortex of a straight-blade VAWT was investigated by using computational fluid dynamics (CFD) and laser doppler velocity (LDV) measurements [14], and several aspects of the flow field were emphasized. An overview of the S4VAWT utilizing three straight blades and a semisubmersible platform was reported by Huijs et al. [15].

Other researchers also focused on the potential of the VAWT for the floating type turbine, among which the floating axis wind turbine (FAWT) is one of the unique concepts in this category [16]. A FAWT consists of a straight-blade VAWT and a spar-type floater that rotate as one. In addition, power take-off (PTO) units are installed on the top end of the spar and then placed above the water surface. The frame of the PTO unit is moored to maintain the FAWT's position and absorb the reaction torque from power generation. This configuration is similar to that of the SeaTwirl [17]. A FAWT positively utilizes the features of VAWTs. Compared to HAWTs, the power coefficient of VAWTs is difficult to reduce when the turbine tilts; thus, a FAWT presupposes its tilt. This results in a smaller spar size and reduced construction costs. In addition, the blades of a FAWT have a feature to furl like an umbrella. This function makes it possible to install the blade at the installation site without a large crane ship. This reduces the installation cost.

Among the numerous research studies done on FOWTs, the numerical approach is considered of value with the quantum progress of the numerical resources. In addition, it is difficult to reproduce the aerodynamics of a full-scale rotor in a model scale because Reynolds number of the model scale is much lower than that of the full scale. Nevertheless, the experimental approach with an ingenious attempt is still useful in understanding the phenomena of a new system, especially for its early stages. Hamedi et al. [18] reviewed experimental methods for FOWTs. Russo et al. [19] conducted an experiment using a 1:40 Froude-scaled spar-type HAWT model whose rotor size was 3.15 [m] and its blade pitch was controllable, to obtain the dynamic loads and its response. They showed the importance of pitch-controlled, variable-speed blades for the dynamics of such HAWTs. The effect of heave plates on the dynamics of a flexible multi-column FOWT was investigated by using the water tank test [20]. Their results showed that the significant height motion of the model with a heave plate decreased approximately 33% under the operational condition, and the decline decreased approximately 66% under the storm and centenary conditions. Robertson et al. [21] conducted model experiments especially focusing on the loads at the low frequencies for a semisubmersible type FOWT. Their data were used for the validation of a numerical model [22]. The dynamic response of the TetraSpar floating wind turbine was investigated using a 1:60 scaled model [23], which included the DTU 10 MW reference wind turbine [24].

The authors of the current study plan to develop a 20 kW FAWT for the first sea trials. Before finalizing its detailed design and sea trials, the dynamics of the updated conceptual FAWT model should be verified by water tank experiments. Akimoto et al. [25] conducted preliminary model experiment using a FAWT model consisting of two parts: the rotor including spar and a supporting floater including PTO. Then, for the simple mechanism, the concept of the FAWT changes so as not to deploy the supporting floater. The motivation of this research is to understand the motion characteristics of the FAWT in several situations. In addition, it also has the motivation to accumulate the motion and mooring tension data for the validation of the upcoming numerical simulation.

2. Methods

2.1. FAWT Model for Water Tank Experiment

The model used in this study was a 1/7.33 scale of the 20 kW FAWT with Froude scaling law. Figure 1 presents the model, and its principal details are shown in Table 1. Stainless beads mixed with water were used as the ballast weight put inside the spar bottom. The total weight of the ballast was 12.8 [kg], and its bulk specific gravity (BSG) was approximately 3.45. This BSG is close to that of crushed rock ballast, and it can be accomplished without any difficulty in actual scenarios.

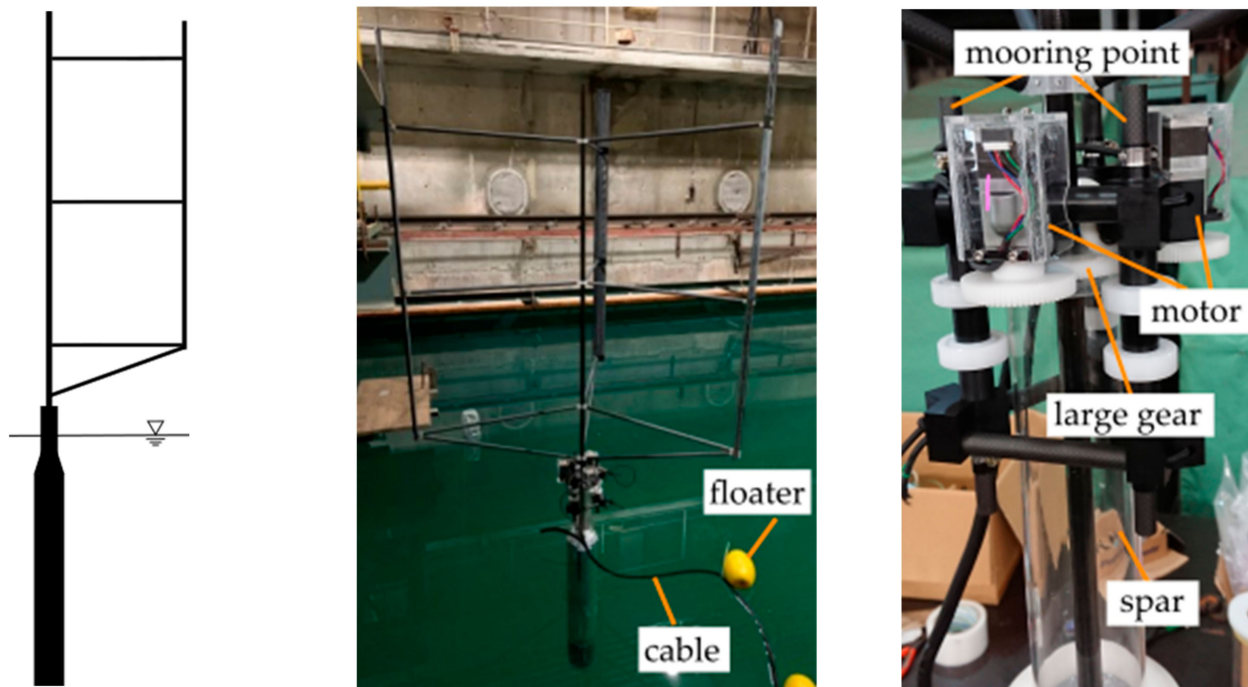


Figure 1. FAWT model for water tank experiment and enlarged view of the rotational mechanism.

Table 1. Principle details of the FAWT model for water tank experiment.

Item	
Height of Rotor, H [m]	1.38
Diameter of Rotor, D [m]	1.38
Number of Blade	3
Blade Cross-section	NACA0021
Blade Chord Length [m]	0.07
Solidity	0.048
Height of Spar [m]	1.42
Diameter of Spar [m]	0.15
Diameter of Spar (slender part)	0.089
Total Height of the model [m]	3.13
Draft [m]	1.28
Total Weight in Air [kg]	20.0
Center of Gravity from bottom [m]	0.34
Center of Buoyancy from bottom [m]	0.57

Meanwhile, reproducing the aerodynamic characteristics of the blades in this scale model experiment can be quite challenging due to the difference in the Reynolds number. Therefore, the evaluation of the aerodynamic characteristics of the FAWT is not the aim of this research. Instead, its goal is to understand the dynamics of FAWT under wind and wave conditions. In particular, the rotor is forced to rotate in a counterclockwise direction by the three regenerative motors, which correspond to the generators in the actual FAWT.

The angular velocities of these motors are controlled by a single controller device and can work in exact synchronization with each other. The cables from the controller to the motors are banded together and in total four floaters are attached to it to adjust its weight in neutral water as shown in Figure 1.

2.2. Experimental Setup

Model experiments were conducted in the towing tank (L [m] × B [m] × D [m]: 100 × 7.8 × 4.35) at Osaka University. The tank has a plunger-type wave maker, but it is not equipped with a blower to generate winds. In this study, a blower was assembled with 24 industrial fans. This was installed on the sub-towing carriage, and its horizontal position could be adjusted along the towing tank. The purpose of this blower was to provide the thrust force on the rotating model and make its tilt angle approximately 20 [deg], which is the assumed tilt angle for the 20 kW FAWT in rated operation. Figure 2 presents the towing tank and the blower.

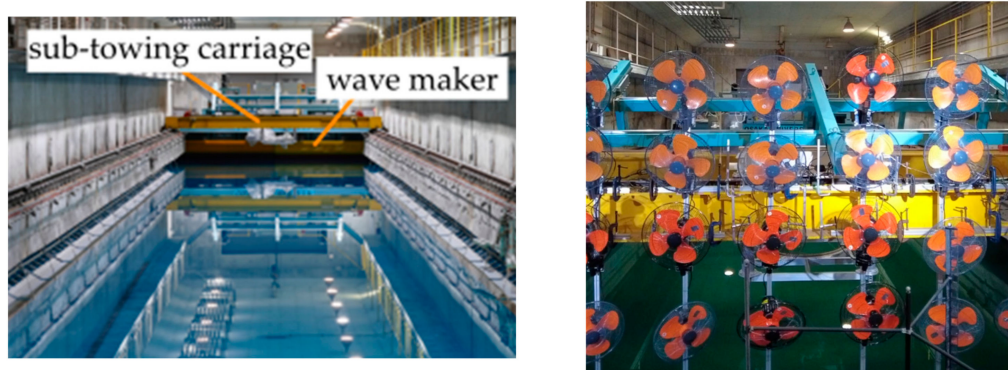


Figure 2. Towing tank (left) and the assembled blower (right).

In the towing tank, the FAWT model was moored by three mooring lines: one for the upwind direction (ML1) and two for the downwind direction (ML2 and ML3) as they are shown in Figure 3. The expanded angles between each mooring line are not equal because of the breadth of the tank. The angle between the mooring lines at the downwind side is 35 [deg]. The mooring line consisted of a polyethylene rope (upper side) and stainless chain (lower side). Its total length was 13.16 [m]. The upper end of the polyethylene rope was connected to the mooring point at the rotational mechanism part via a ring gauge for taking mooring tension measurements. Meanwhile, the bottom end of the stainless chain was connected to an anchor, whose weight was 5.0 [kg]. For the identification, the lines were numbered in a counterclockwise order from the line to the upwind direction. Table 2 shows the specification of the mooring lines.

Table 2. Specifications of the mooring lines.

Item	
Length of polyethylene rope [m]	3.16
Weight of polyethylene rope per unit length [kg/m]	0.003
Length of stainless chain [m]	10.0
Weight of stainless chain per unit length [kg/m]	0.147

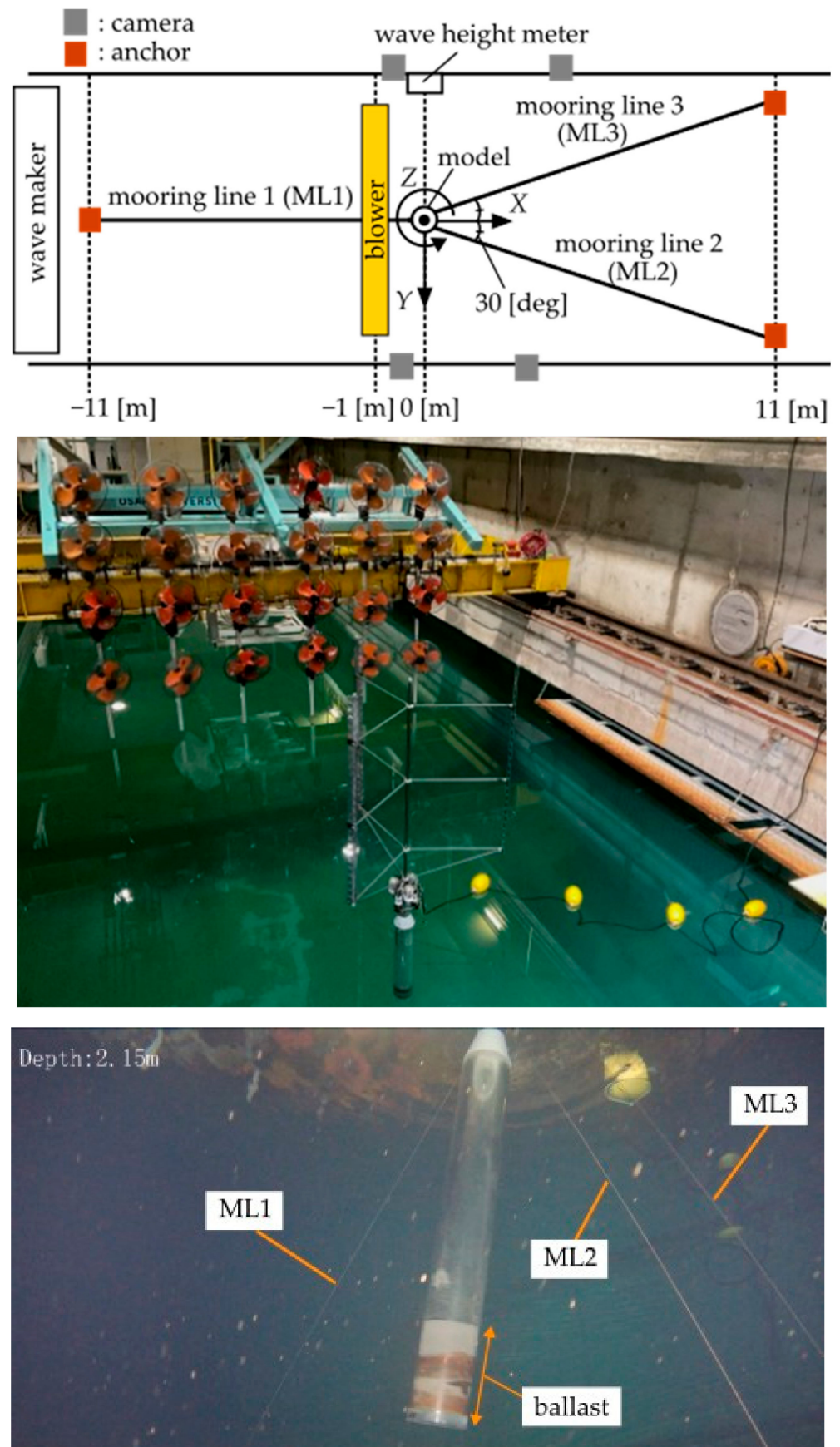


Figure 3. Overview of the experimental setup and photos of the model.

In the present research, six degrees of the FAWT model motion were measured by using an optical tracking system. This system utilized the infrared light emitted from the camera and the reflected infrared light from the target marker. A marker was attached to the upper end of the center shaft and each rotor blade, and four markers were used for the motion measurement. Additional markers were placed on the motor cases for the rotational mechanism. However, such additional markers could not be easily recognized by cameras because they are frequently behind the rotating blades and struts. Therefore, a virtual marker was created by using the function of motion capture software (Motive 2.1.2) and attaching it to the center shaft of the rotor near the rotational mechanism. The translation responses at this virtual marker are less affected by the model rotation because the rotational center of the model is at the rotational mechanism in which the mooring points are located. The direct distance between the marker on the center shaft top and the virtual marker was approximately 1.645 [m]. The rotor tilt was calculated from the motion of these two markers. Four cameras were placed at the catwalk of this towing tank. A wave height meter was then installed at the sidewall of the towing tank so as to measure the wave conditions at the model's initial position. Thus, the measured items were the motion of the model, wave height, and mooring tensions. The sampling frequency of each item was 100 [Hz] and a trigger signal was used to synchronize these measured data. Figure 3 presents the experimental setup with the coordinate system for the motion tracking and photos. As can be seen, the origin of the coordinate system is on the initial position of the virtual marker, and the +Z axis is the upward direction.

2.3. Experimental Conditions

Wave conditions were fixed by using the data from the Nationwide Ocean Wave information network for Ports and HARbourS (NOWPHAS) [26]. The authors assumed the wave conditions for a 20 kW FAWT under the operating limit and extreme condition, and they were converted into the model scaled with the Froude similarity law. Table 3 shows these values.

Table 3. Wave conditions for the 20 kW FAWT and 1/7.33 scale model.

Operating Limit	20 kW FAWT	Scale Model
Significant wave height [m]	0.5	0.068
Mean wave period [s]	7.5	2.77
Extreme Condition	20 kW FAWT	Scale Model
Significant wave height [m]	1.0	0.136
Mean wave period [s]	13.0	4.80

The maximum wavelength that could be generated by the wave maker was 20 [m], and it assumed the deepwater wave. The wavelength λ [m] corresponding to the wave period in Table 3 can be calculated using the following equation:

$$\lambda = \frac{gT_W^2}{2\pi} \quad (1)$$

where g [m/s²] is gravity acceleration, and T_W [s] is the wave period.

As described in the previous section, the model proposed in this research was forced to rotate by three motors. The wind velocity at 1.0 [m] apart from the blower was approximately 2.0 [m/s]. This velocity was approximately 5.4 [m/s] in the actual situation by the Froude similarity law. However, this velocity is not a meaningful value because, in this research, the purpose of the velocity from the blower is to make the rotating model inclined. Here, we assumed that it takes 60 [s] to achieve stable winds. Under this wind velocity condition, the model tilt angle could be adjusted by turning the angular velocity of three motors. Then, 70 [rpm] (7.33 [rad/s]) was adopted for the angular velocity of the model. The mean tilt angle was approximately 17 [deg] under these conditions.

Apart from the fundamental experiments to obtain the natural periods and response amplitude operator (RAO) of the model, several situations that the FAWT would face in actual sea conditions were assumed and examined in this research. Such situations, along with their explanations and purposes, are presented below.

- (1) regular waves: RAO of the FAWT (parking or operating)
- (2) irregular waves: response of the FAWT (parking or operating)
- (3) rapid decrease of wind velocity: wind velocity changes from 2.0 to 0.0 [m/s]
- (4) transient response in start-up: number of rotations changes from 0 to 70 [rpm]
- (5) transient response in shutdown: number of rotations changes from 70 to 0 [rpm]
- (6) unbalanced blades weight: an additional weight is attached on the top of one blade
- (7) passive braking system for rotor over speed: drag parts are attached on the spar
- (8) damaged case: one block of the spar near the sea surface is assumed to be flooded

Based on the values in Table 3 and the limitation of the wave maker, the wave conditions for the above situations are fixed. Table 4 shows the experimental conditions. In the table, P and O indicate parking and operating, respectively. In addition, R and I indicate regular and irregular waves, respectively. Here, the International Towing Tank Conference (ITTC) wave spectrum was used for the irregular waves, while the wave height and period in the table correspond to the significant wave height and mean wave period.

Table 4. Experimental conditions.

Case	Rotor	Wave	Wave Height, H_w [m]	Wave Period, T_w [s]
(1)	P	R	0.05	2.68, 2.86, 2.95, 3.04, 3.12, 3.20, 3.30, 3.40, 3.49, 3.58
	O	R	0.05	2.68, 2.86, 2.95, 3.04, 3.12, 3.20, 3.30, 3.40, 3.49, 3.58
(2)	P	I	0.068, 0.136	2.77
	O	I	0.068, 0.136	2.77
(3)	O	R	0.068	3.04, 3.40, 3.58
(4)	P→O	R	0.068	3.04, 3.40, 3.58
(5)	O→P	R	0.068	3.04, 3.40, 3.58
(6)	O	R	0.05	3.40
(7)	O	I	0.068	2.77
(8)	P	R	0.05	2.68, 2.86, 2.95, 3.04, 3.12, 3.20, 3.30, 3.40, 3.49, 3.58
				3.30, 3.40, 3.49, 3.58

3. Experiment Results and Discussions

3.1. Decay Tests

Natural periods of the model were obtained by using decay tests. Adequate initial displacement or inclination was given to the model. Then, the model was released, and the model motion was measured. Each test condition was conducted three times, and the mean values were used as the natural periods. Figure 4 presents the time histories of model responses at the virtual marker. Compared with the sway direction, it is difficult to make a pure surge initial displacement due to the mooring direction. Therefore, the effect of pitch was observed in the beginning of the surge time history. Table 5 shows the measured natural periods of the model and their converted values in the 20 kW FAWT scale. Note that the values for the 20 kW FAWT scale are rough indications because the configuration of the FAWT model used in this research is simplified and the expanded angles between each mooring line will be equal at sea. Compared with the natural period of surge, that of the sway direction is long, which could be due to the small restoring force from the mooring lines in the Y direction and the variations with the directions of the ML2 and ML3 shown in Figure 3. The natural period of the 20 kW FAWT in the heave direction is slightly close to the significant wave period shown in Table 3. To avoid the resonance phenomenon, it is necessary to decrease the water-plane area or attach a heave plate at the bottom of the spar for the 20 kW FAWT.

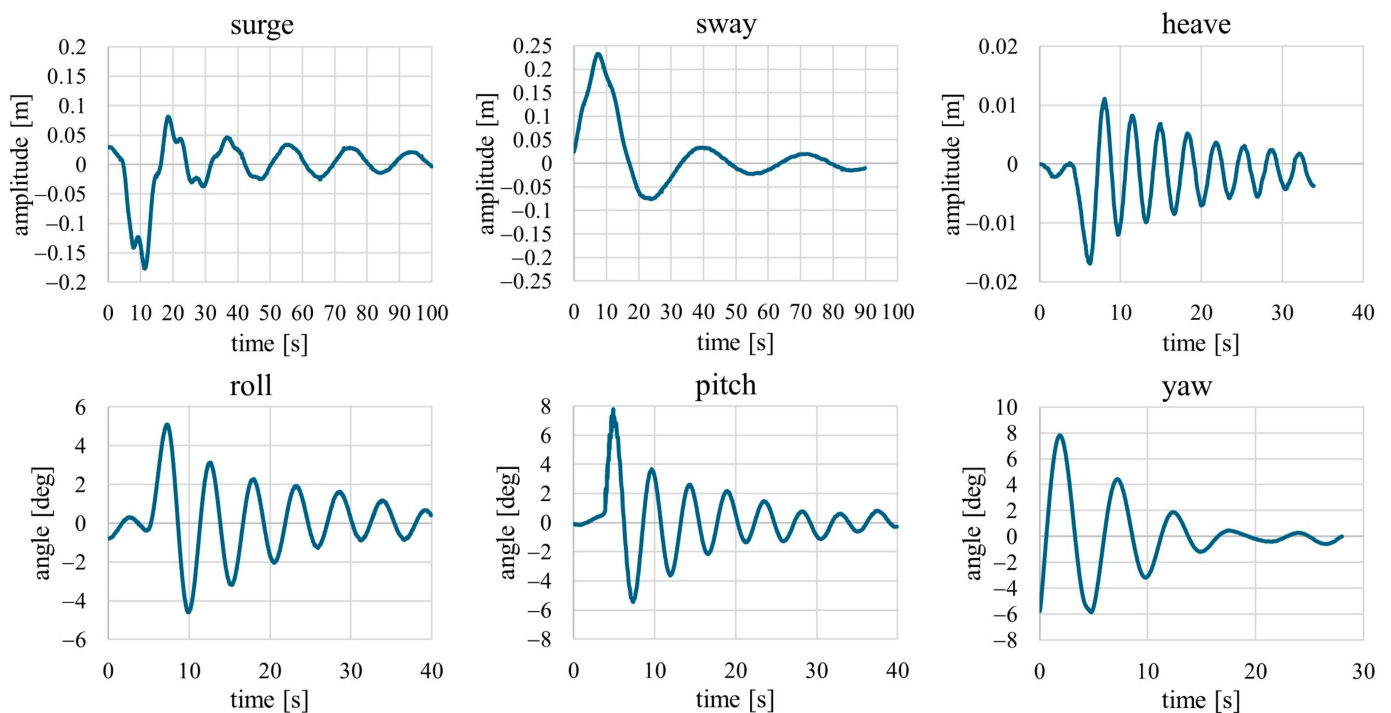


Figure 4. Time histories of the model in decay test.

Table 5. Natural periods of the FAWT model and 20 kW.

Direction	Scale Model	20 kW FAWT
Surge	20.5	55.5
Sway	32.8	88.8
Heave	3.4	9.2
Roll	5.1	13.9
Pitch	4.6	12.3
Yaw	5.1	13.9

unit: [s].

3.2. RAO of the FAWT

The RAOs were obtained from the time histories of model motion under the wind and wave conditions. The mean amplitude of model motion was normalized by the incoming wave amplitude 0.025 [m] for surge, sway, and heave. Meanwhile, the mean angle of inclination in each axis was normalized by the incoming wave slope angle θ_w [rad], which we calculated using Equation (2):

$$\theta_w = \tan^{-1} \left(\frac{\frac{1}{2} H_w}{\frac{1}{4} \lambda} \right) \quad (2)$$

Figure 5 presents the RAO results. Concerning the surge direction, the RAO of the operating FAWT is smaller than those of the parking condition. Under the operating condition, thrust force to downwind direction is generated by the rotor. This thrust is borne by the mooring line at upwind side ML1, and its tension increases. As a result, the surge motion becomes small. As shown in Table 5, the natural period of heave is 3.4 [s] in the model scale. Around this period, the heave RAO of the model is approximately 1.3. Although the floating platform of the FAWT is relatively small compared with its rotor size, its heave RAO is not so much different from the other experimental results using different floating platforms: 2 MW semisubmersible type [27], 5 MW spar type [28], and 7 MW V-shaped semisubmersible type [29]. The difference between the parking and operating conditions is that the resonance period of the operating FAWT shifts to the shorter wave

period side. This can be explained by the increase in the water-plane area. In the case of the operating FAWT, the rotor inclines to the downwind side by the thrust force, resulting in the increase of the water-plane area. Then, the restoring force in the heave direction increases with the water-plane area, and the resonance period is shifted. Additionally, the bottom parts of the rotational mechanism submerge under the operating condition, which also increases the water-plane area and the restoring force. However, the submergence of the rotational mechanism frame occurs only in the model scale, because the size of that part becomes relatively big compared with that of the 20 kW FAWT. As for the pitch and roll RAOs, those under the operating condition were smaller than those under the parking condition because of the rotor's gyroscopic effect.

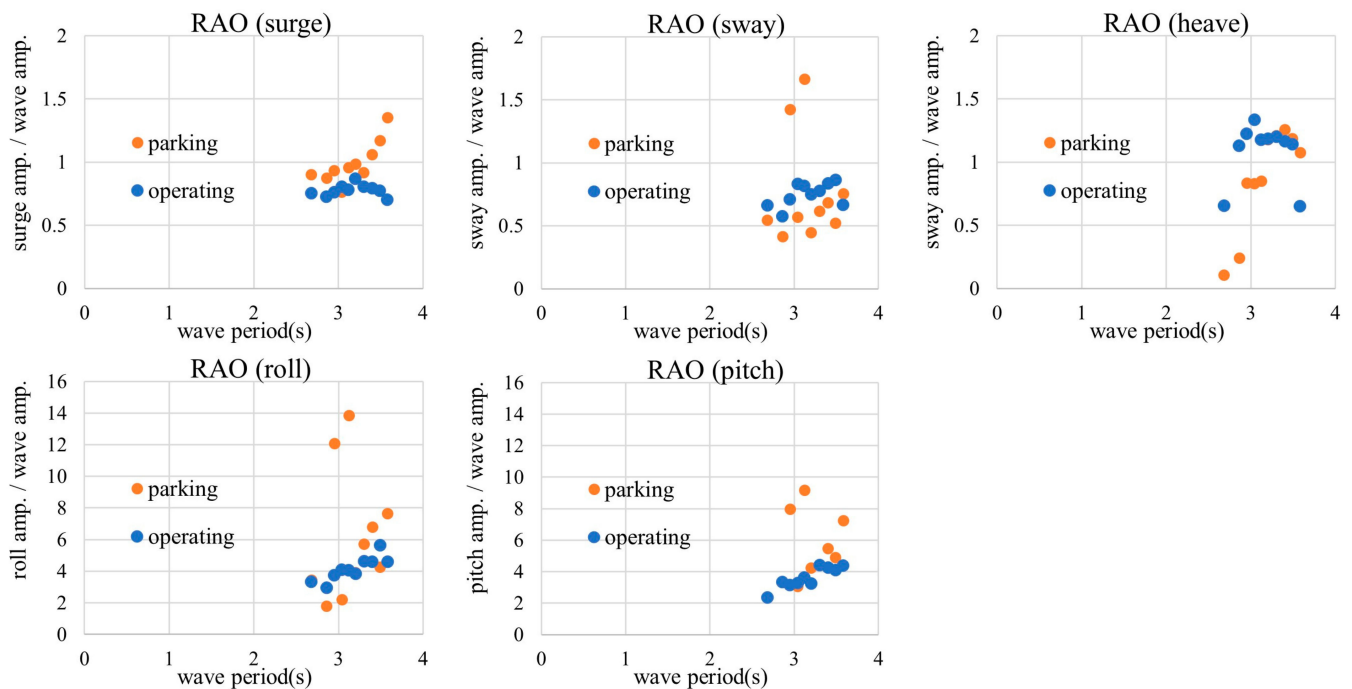


Figure 5. RAOs of the FAWT under the parking and operating conditions.

3.3. Response of the FAWT under the Irregular Waves

In this experiment, we verified the responses of the parking or operating FAWT under the irregular waves and steady wind. Examples of the time histories of the response and mooring tensions for the operating FAWT are shown in Figure 6. The significant wave height and mean wave period are 0.136 [m] and 2.77 [s], respectively. As shown in the time histories of the responses, there is no strange behavior that can be observed in the measured data. A correlation can be seen between heave and wave height. The oscillation center of heave motion shifts downward by approximately -0.02 [m]. This is because ML1, whose tension increases against the thrust force from the rotor, draws the model into the water. The steady pitch angle is approximately 13 [deg], which is mainly caused by the thrust force from the operating rotor in the wind. Apart from the steady pitch angle, we also observed the irregular pitch oscillation caused by the incoming irregular wave. Compared with the heave, the correlation between pitch and wave height is not so strong because the natural period of pitch is longer than that of heave. Table 6 presents the maximum amplitude of heave normalized by a half of the significant wave height and the maximum pitch angles. Under these irregular wave conditions, the heave amplitude corresponds to the significant wave height is approximately 1.0. Furthermore, excessive inclination does not occur.

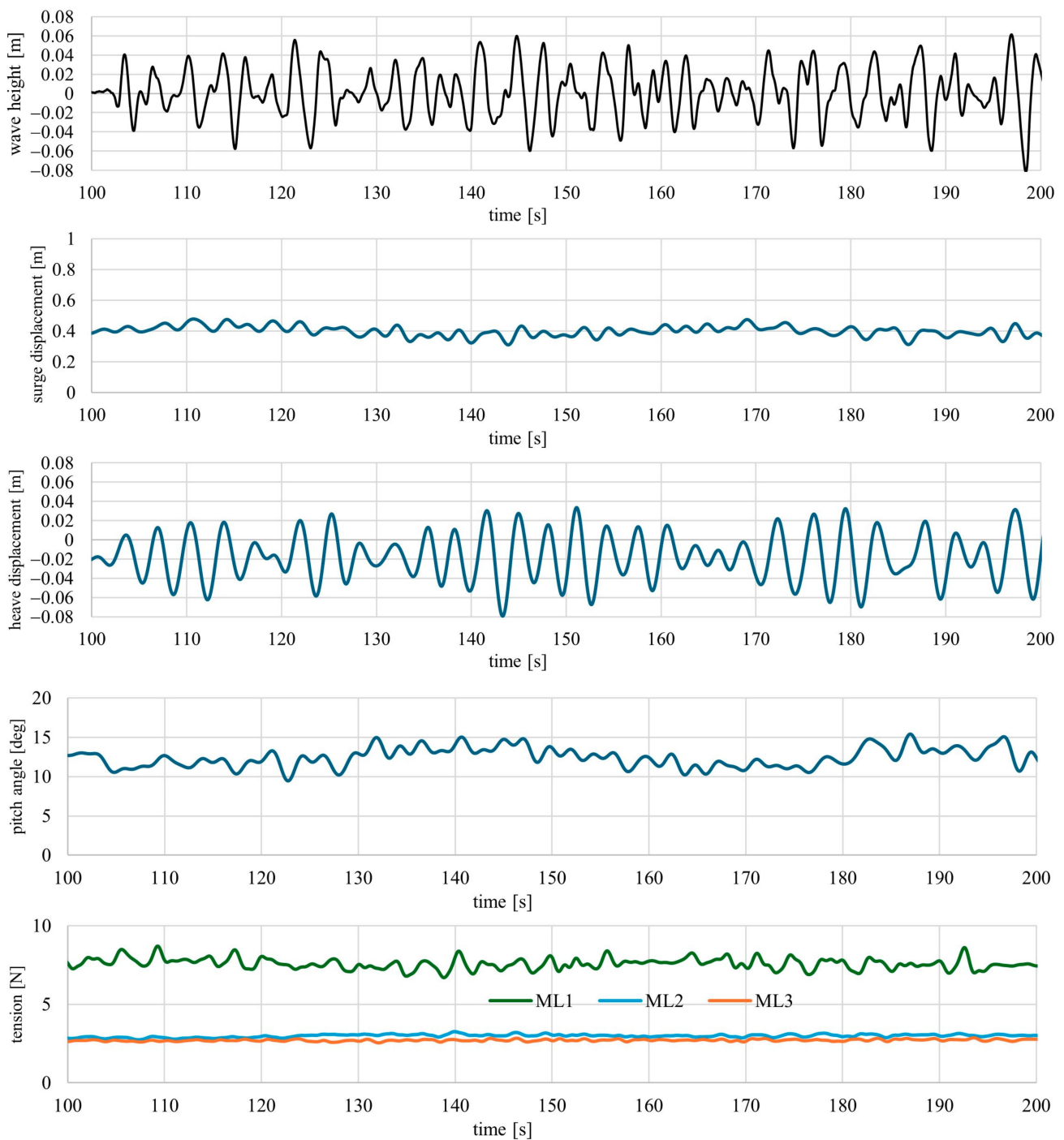


Figure 6. Time histories of the wave height, surge, heave, pitch, and mooring tensions.

Table 6. Normalized maximum heave amplitude and pitch angle.

H_w [m]	Wave Condition		Rotor	Normalized Max. Heave Amplitude [-]	Max. Pitch Angle [deg]
	T_w [s]				
0.068	2.77	Parking		0.85	8.0
		Operating		1.01	16.1
0.136	2.77	Parking		0.89	10.0
		Operating		0.81	16.1

As for the time histories of the mooring tensions, irregular fluctuations are observed in the three mooring lines. The tension of ML1, which tenses by the thrust force acting on the rotor, increases from the initial one. Meanwhile, the tensions of the ML2 and ML3, which are located at the downwind side, decrease compared with their initial tensions because they are loosened according to the model motion in the +X direction. Table 7 shows the maximum mooring tension for ML1 and mean mooring tension for ML2 and ML3, which are normalized by their initial mooring tensions. The initial mooring tension, which is measured at the beginning of each experiment, indicates the tension in still water and the no-wind condition. As shown in the table, the maximum tension of ML1 to the upwind side is approximately twice the value of its initial one under the operating condition. Concerning the mooring lines to the downwind side, the decrease ratio from its initial tension is approximately 10–20%. The tension of ML2 is slightly bigger than that of ML3 because ML3 is loosened compared with the ML2. In this research, the rotational mechanism rotates the rotor counterclockwise, as viewed from above, while the reaction torque from the rotor rotates the rotational mechanism in a clockwise direction.

Table 7. Maximum or mean tensions normalized by the initial tensions.

Wave Condition		Rotor	ML1	ML2	ML3
H_w [m]	T_w [s]				
0.068	2.77	Parking	1.36 (4.58)	0.96 (3.12)	0.92 (3.51)
		Operating	2.02 (4.57)	0.92 (3.13)	0.77 (3.49)
0.136	2.77	Parking	1.53 (4.56)	0.97 (3.14)	0.93 (3.49)
		Operating	2.00 (4.57)	0.92 (3.26)	0.78 (3.49)

Values in parentheses are the initial mooring tensions [N].

3.4. Response under the Rapid Decrease of Wind Velocity Condition

In this experiment, the model was initially rotated at a constant speed (7.33 [rad/s]) in the wind velocity at 2.0 [m/s] and regular waves. Then, the wind velocity was rapidly decreased to zero by turning off the blower. The model response and the mooring tensions were measured during this transition phase. In this phase, the angular velocity of the model was kept constant because the operating FAWT kept its angular velocity for a while by its inertia if the wind suddenly decreased in the actual condition. Figure 7 presents an example of the time histories of the model response and mooring tensions. In the figure, the red line indicates the time when the wave maker got started, while the purple line indicates the time when the blower was turned off. It takes approximately 20 [s] to reach the calm condition after the blower is turned off because of each fan's inertia.

The surge displacement is mainly caused by the thrust force from the rotor. After the blower is turned off, the displacement gradually decreases. The heave amplitude is slightly increased, and the center of oscillation in the heave response slightly shifts to the upward direction because of the decreased ML1 tension. The pitch angle, which is mainly caused by the thrust force from the rotor, gradually decreases. Then, the only oscillation caused by the waves is dominant in pitch response. The ML1 mooring tension gradually decreases with decreasing thrust force from rotor, and it oscillates with the wave forces on the spar. Meanwhile ML2 and ML3 tense up, and their mooring forces increase. Notably, there are no unsafe model responses in this rapid decrease of the wind velocity from the rated condition.

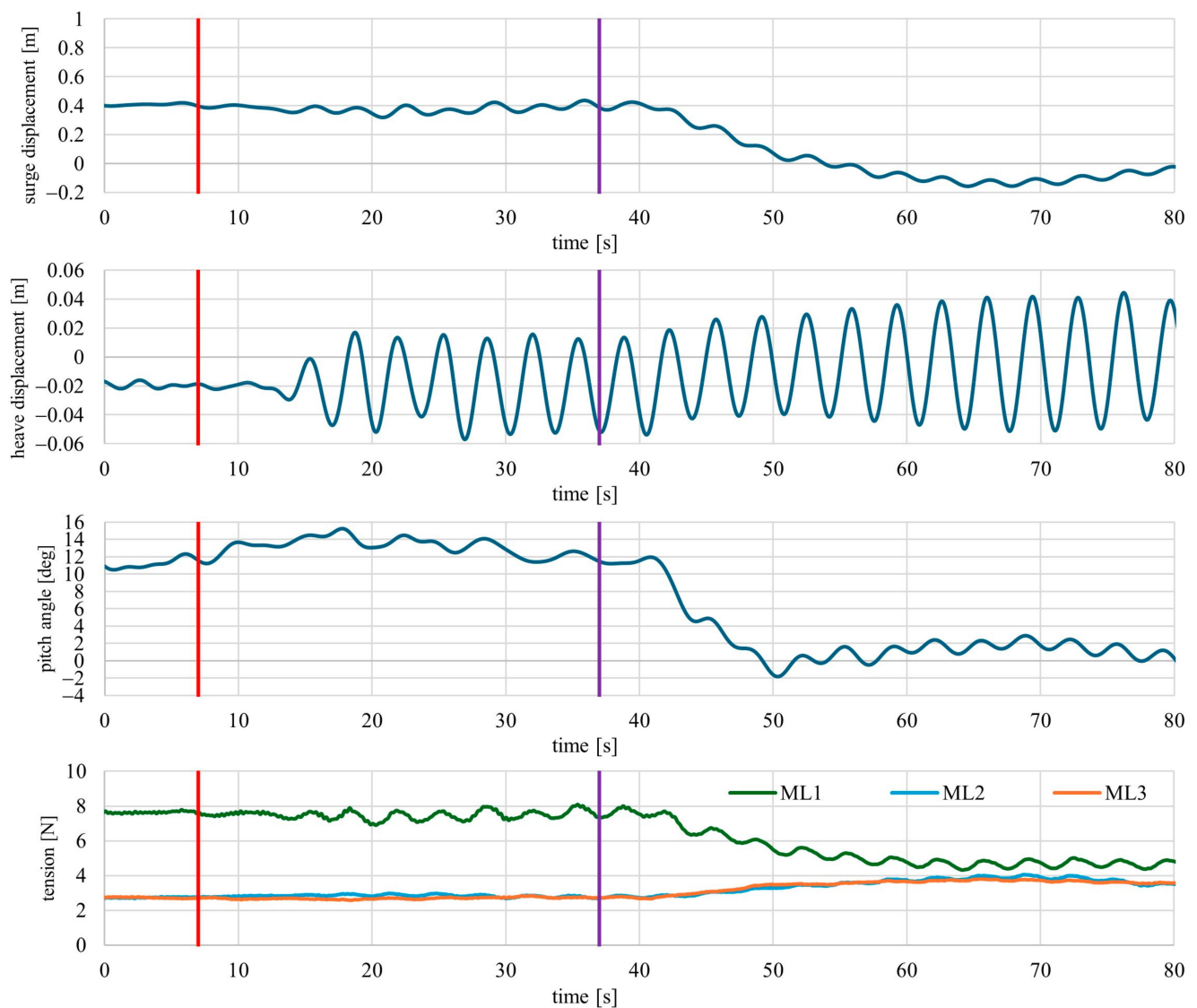


Figure 7. Time histories of model response and mooring tensions during the wind velocity decrease. (red line: the wave maker got started, purple line: the blower was turned off).

3.5. Transient Response in Start-Up or Shutdown

The responses during the start-up or shutdown conditions were verified in this experiment. For the start-up process, the model was initially exposed to the steady wind and regular waves. Then, the model's angular velocity increases to the target value (7.33 [rad/s]) from 0, with the constant angular acceleration of $0.25 \text{ [rad/s}^2\text{]}$. It takes approximately 30 [s] to make the angular velocity increase from zero to the target value. As for the shutdown process, the initial condition is that the model must be rotating with the constant angular velocity (7.33 [rad/s]) under the steady wind and regular waves. Then, the model's angular velocity decreases to 0 with the same constant angular acceleration. Figures 8 and 9 present examples of the time histories of measured data for the start-up and shutdown condition, respectively. The red line indicates the time when the wave maker gets started, while the purple line indicates the time when the rotor starts to increase or decrease the angular velocity. The blower works at all times. This leads to steady surge displacement and pitch angle values at approximately 0.2 [m] and 4 [deg], respectively, before the start-up and after the shutdown process. Meanwhile, the thrust force acting on the rotor varies with the angular velocity of the rotor. As for the start-up process, the model position shifts to the downwind side (+X direction) and is drawn into the water ($-Z$ direction) after the

rotor starts to increase the angular velocity. Moreover, the pitch angle and tension of ML1 both increase. Thus, we have confirmed that the converse phenomenon occurs between the start-up and shutdown process and that there are no unsafe model responses during these processes.

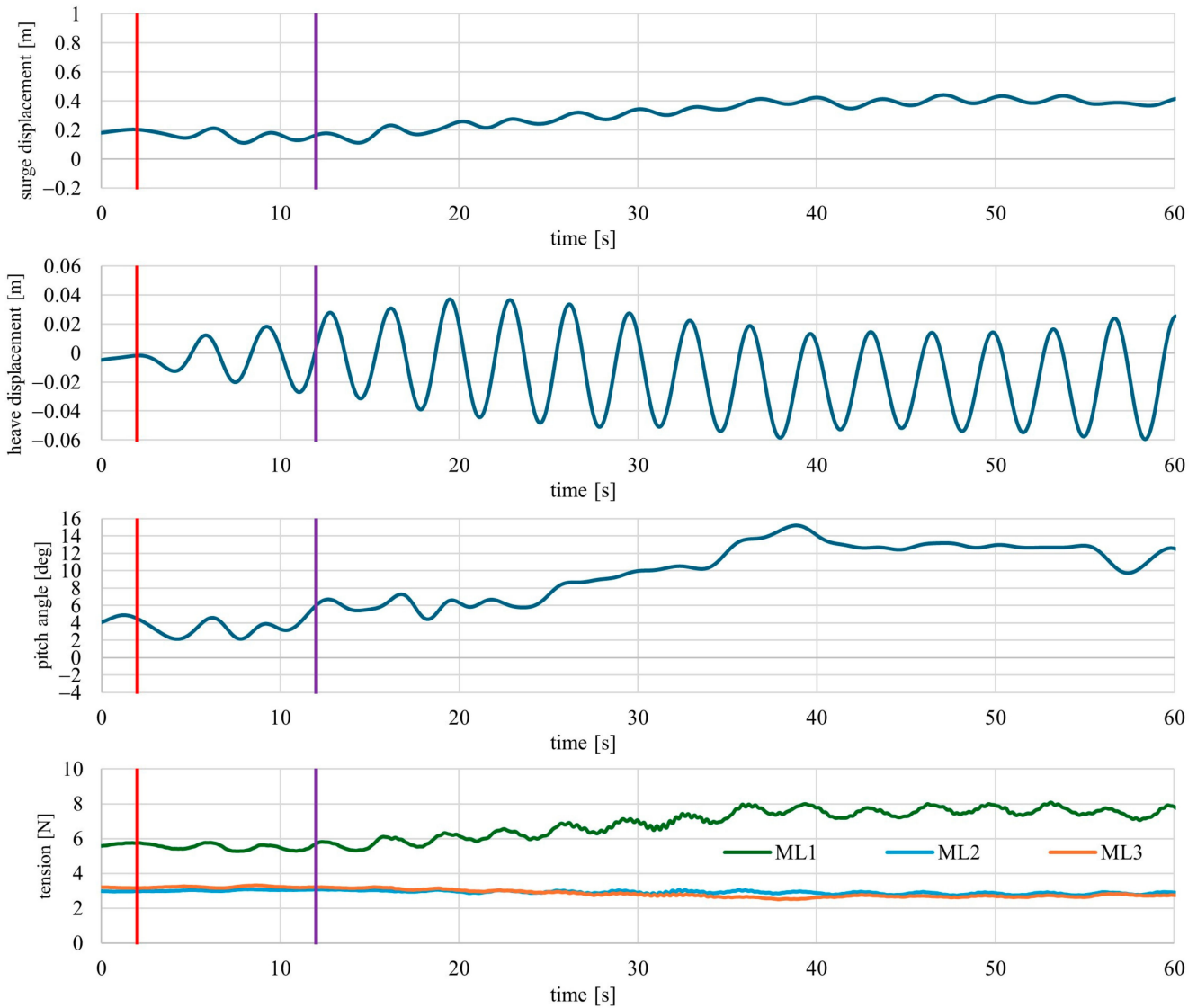


Figure 8. Time histories of model responses and mooring tensions during the start-up process. (red line: wave maker gets started, purple line: the rotor starts to increase its angular velocity).

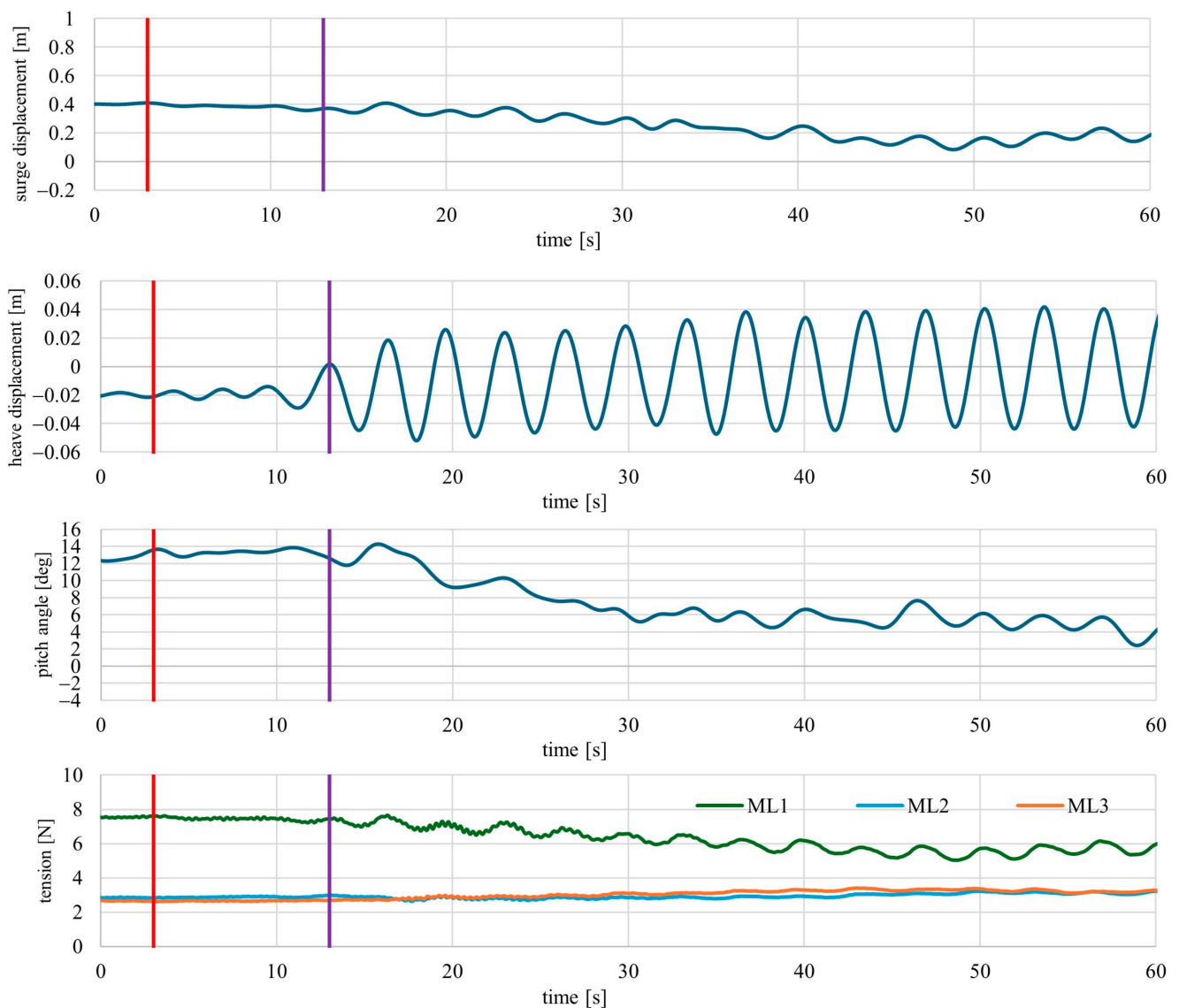


Figure 9. Time histories of model responses and mooring tensions during the shutdown. (red line: wave maker gets started, purple line: the rotor starts to decrease its angular velocity).

3.6. Unbalanced Blades Weight Case

We adequately adjusted the weight of each blade so as not to make the center shaft vibrate during operation. However, the response when the weights of the blades get thrown off-balance due to accidents, such as a bird strike or accumulated snow, should be verified. In this experiment, an additional weight was attached on the top of one blade, and the transient response of the model was measured throughout the process from start-up to shutdown. The additional weight of 25 [g] was approximately 10 [kg] in the 20 kW FAWT scale. Next, the measured data were divided into two separate terms. One is from the start-up to normal operation, and the other is from normal operation to shutdown. Figure 10a presents the time histories of the center shaft top in the X and Y direction for the former part, and Figure 10b presents those for the latter part. In the figure, the purple line indicates the time when the rotor starts to increase or decrease the angular velocity. Figure 11 presents the Fast Fourier Transform (FFT) response of the time histories between 35~135 [s], which are shown in Figure 10a,b. From these figures, it is confirmed that short-period motion occurs in both the X and Y direction in case of the model with additional weight. Its frequency is approximately 1.16 [Hz] as shown in Figure 11 and corresponds to the angular velocity of the rotor (7.33 [rad/s]). Figure 12 presents the trajectories of the top of the center

shaft in the horizontal plane. The data for this figure correspond to Figure 10a,b. The initial position of the center shaft is the origin, and the wind direction is from $-X$ to $+X$. There is no large difference between the total displacements in the X direction with and without additional weight. However, the trajectory with additional weight forms a circle, and it is confirmed that the additional weight causes a slewing motion. The effect is quite noticeable in the shutdown process where the gyro effect becomes diminished. The radius of this slewing motion is approximately 0.05 [m], which is approximately 0.37 [m] in the 20 kW FAWT scale. The stiffness of the center shaft is lowered with the growing size of the rotor and the weight saving. Obviously, it is important to maintain the adequate weight balance of the blades.

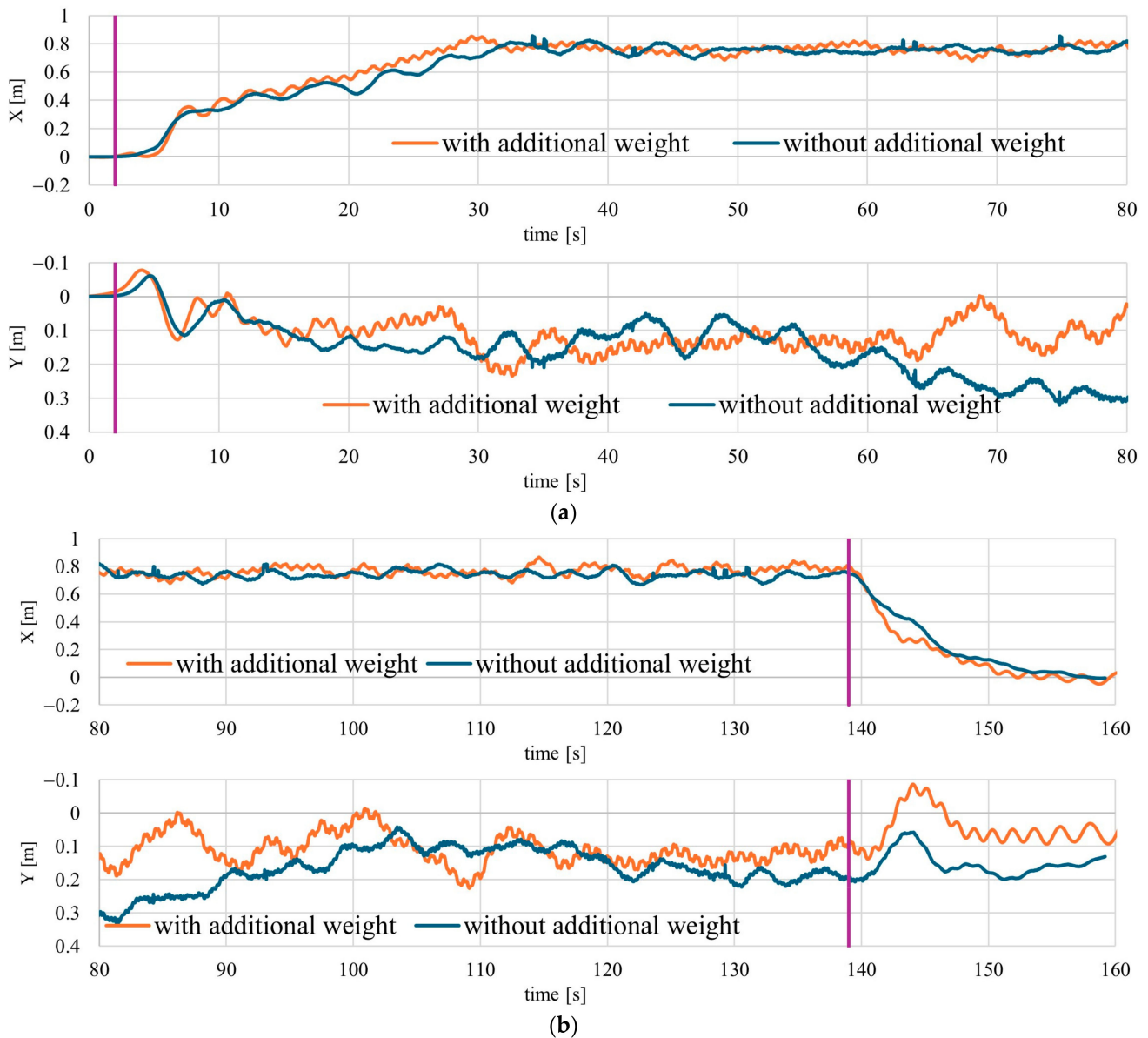


Figure 10. (a) Time histories of the top of the center shaft in X and Y direction from start-up to normal operation. (purple line: the rotor starts to increase), (b) Time histories of the top of the center shaft in X and Y direction from normal operation to shutdown (purple line: the rotor starts to decrease its angular velocity).

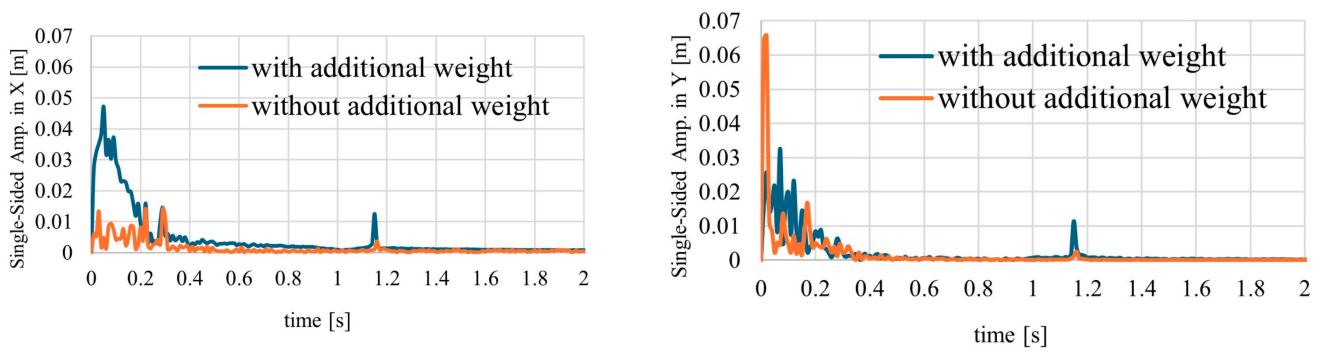


Figure 11. FFT response of the center shaft displacement in X and Y direction.

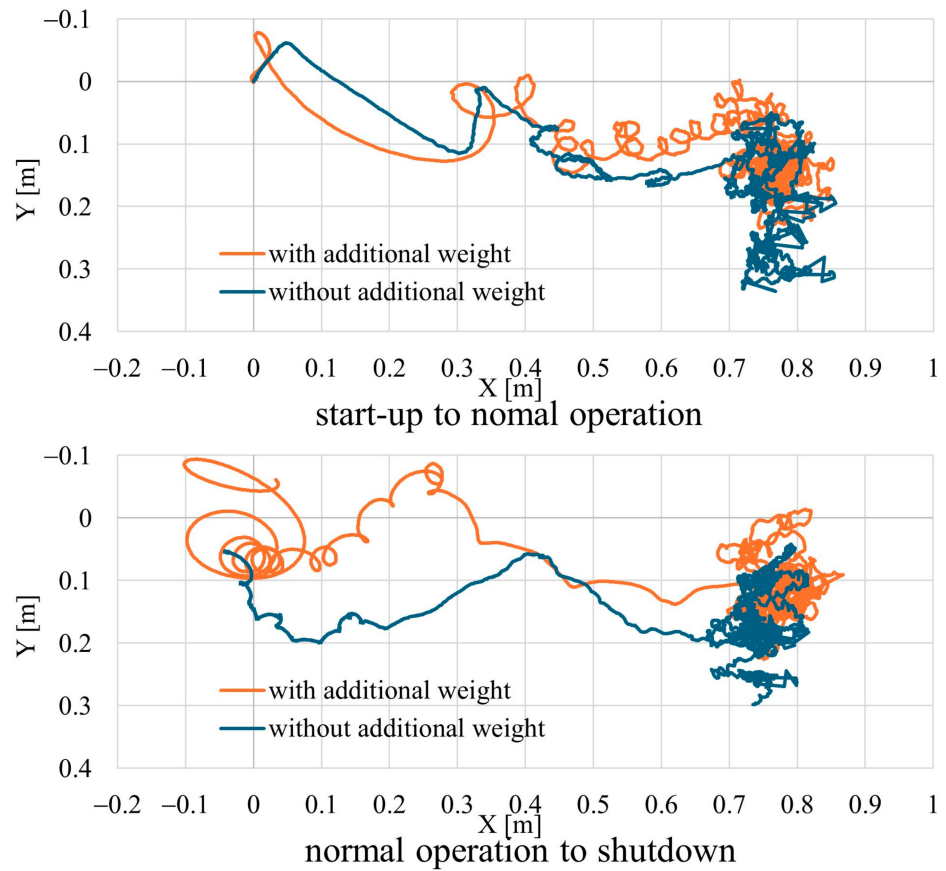


Figure 12. Trajectories of the top of the center shaft (upper: start-up to normal operation, lower: normal operation to shutdown).

3.7. Passive Braking System for the Rotor Overspeed

Overspeed control of the rotor is one of the important challenges for the VAWT. The use of an appendage that becomes submerged in the water only when the overspeed occurs is a simple method to passively decrease the rotational speed. Under the rated operation, the FAWT inclines due to the thrust force of the rotor and is drawn into the water by the tension of the upwind side mooring line. The appendage will be installed to the slender part of the spar located above the water surface and below the frame of the rotational mechanism. Figure 13 presents the appendages used in this experiment and a photo of the spar part installed on them. The installed appendages are constantly in the water because the frame of the rotational mechanism is relatively long for the model.



Figure 13. Photos of the appendages and the spar installed on them.

As previously mentioned, in the current study, the rotor is forced to rotate by three motors with the rotational speed control (not the torque). Therefore, the rotational speed is kept constant, and the mooring tension increases when the appendage submerges and rotates in the water. Figure 14 presents the time histories of the mooring tension with and without the appendages. The wave condition is an irregular wave, with average wave height and mean period of 0.068 [m] and 2.77 [s], respectively. The mooring tension of ML1 for the model with appendages increases compared with that of the model without the appendages. This indicates that the drag force on the appendages increases the rotational torque of the FAWT as expected. This experimental result confirms that this simple brake system with appendage works when submerged under the over speed condition. However, the excessive torque increase causes the situation wherein the spar winds the mooring lines. Thus, adequately sized appendages should be installed if this passive braking system is applied.

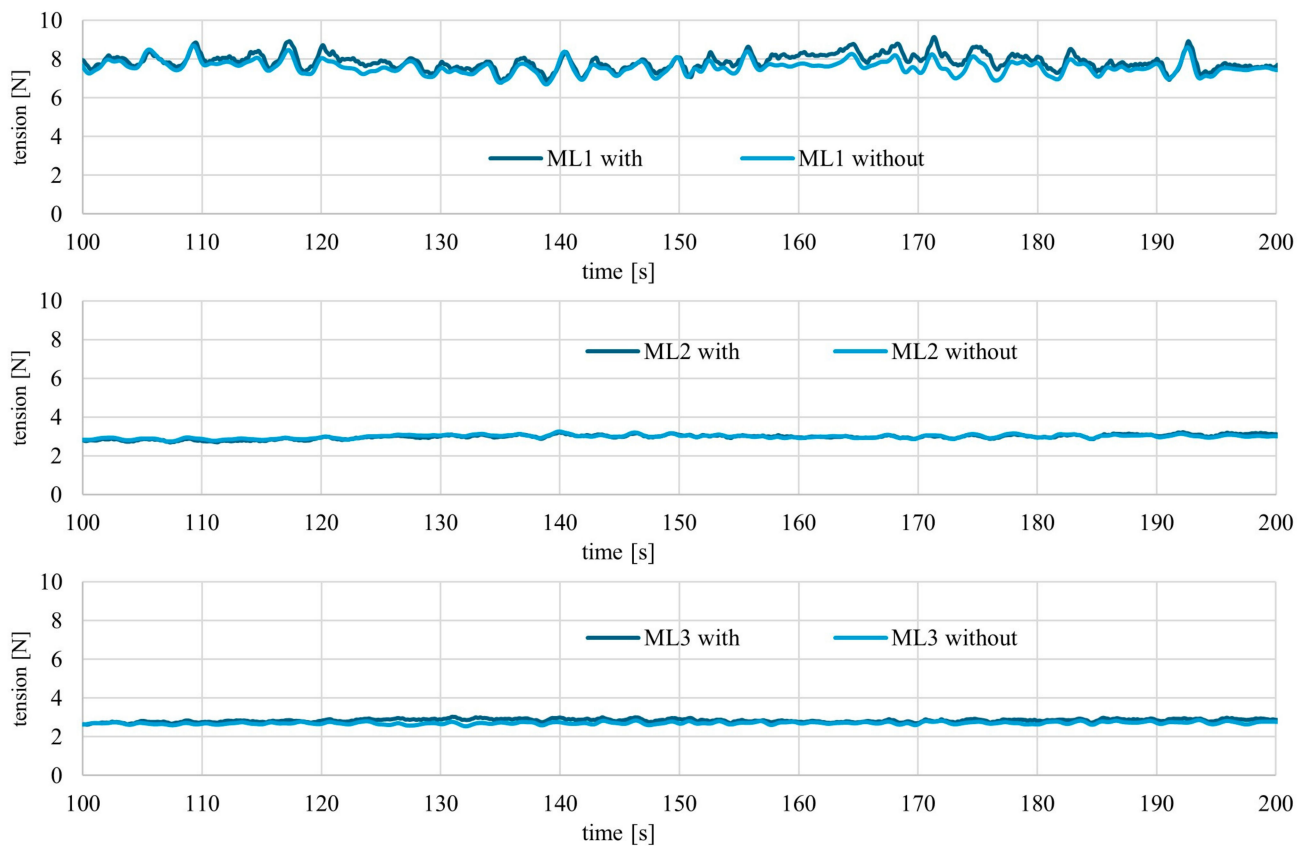


Figure 14. Time histories of the mooring tensions for the model with and without the appendages.

3.8. Damaged Case

Under the survival condition, it is assumed that a floating object hits the spar part of the parking FAWT. At that time, one block of the spar near the sea surface (slender part) may be flooded. The slender part of the spar is segmented in the vertical direction for the 20 kW FAWT, and the length of one block is assumed as 0.7 [m]. The amount of the decreased buoyancy is approximately 2.3 [N]. In this experiment, we attached additional 0.6 [kg] weights to the bottom of the rotational mechanism frame to reproduce this condition. As a result, the settlement of the model is approximately 0.08 [m]. Figure 15 presents the draft of the model with and without the additional weights. Furthermore, the red line in the figure indicates the water line. It is confirmed that the bottom part of the rotational mechanism is submerged for the damaged case.

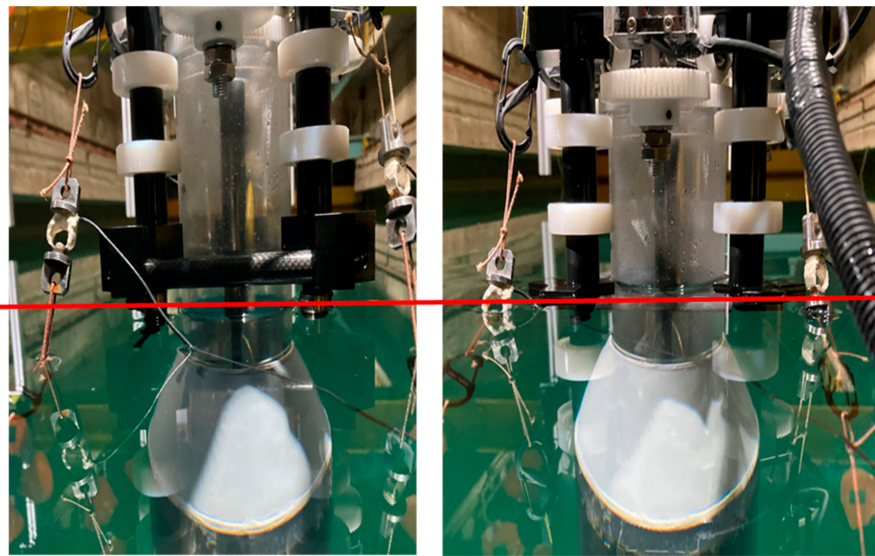


Figure 15. The draft of the model with (right) and without (left) the additional weights. (red line indicates the water line).

Meanwhile, Figure 16 presents the RAOs of the damaged model and those of the harmless model, as shown in Figure 5. The resonance period of the damaged model shifts to the shorter side, and its response amplitude becomes small for heave. The pitch angle of the damaged model also becomes smaller compared with the harmless model, which may be attributed to the increase of the water-plane area and damping force caused by the bottom frame submergence of the rotational mechanism. This rotational mechanism, which corresponds to the PTO of the 20 kW FAWT, becomes relatively large for the model used in this research. A relatively small PTO could be designed for the 20 kW FAWT that will not submerge under the operating condition. However, in the damaged case, there is an advantage if the bottom of the PTO part submerges to ensure safety.

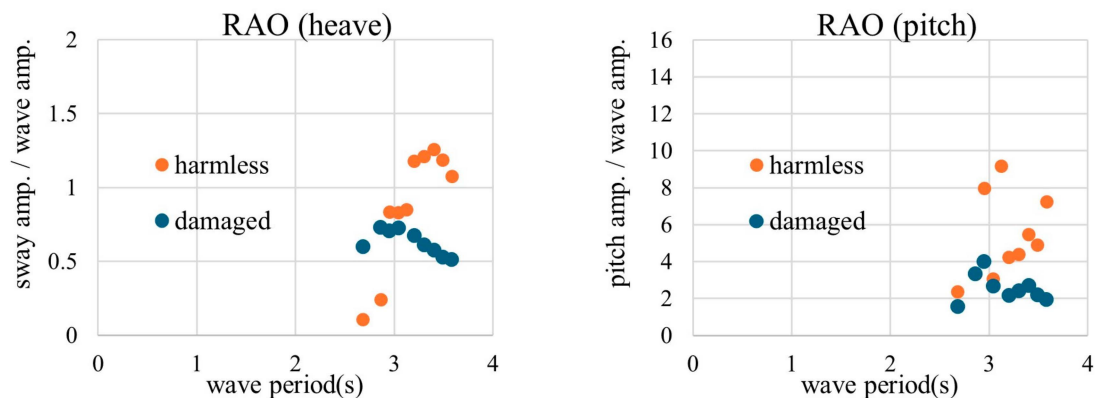


Figure 16. RAOs of the damaged and harmless FAWT under the parking condition.

4. Conclusions

In this study, the dynamics of a FAWT were investigated experimentally using a scale model moored in the water tank with three mooring lines and exposed to wind and wave. The purpose of the wind is to steadily tilt the model to the downwind direction when the FAWT operates, while the wind velocity is not set to a certain velocity. The following conclusions can be drawn from the experimental results:

- The heave RAO of the FAWT model is approximately 1.3—a value that is comparable to those of the other FOWTs, whose floaters are relatively large compared with that of the FAWT.
- Pitch and roll RAOs under the rated operation are smaller than those under the parking condition due to the rotor gyroscopic effect.
- Under the irregular waves, normalized heave amplitude by the incoming significant wave height is approximately 1.0.
- In case of the operating FAWT under irregular waves, the maximum tension of the mooring line to the upwind side is approximately twice of its initial one in still water. Meanwhile, the mean tensions of mooring lines to the downwind side decrease by approximately 10–20% percent from their initial ones.
- A sudden decrease of incoming wind does not affect the dynamics of the operating FAWT because of its inertia.
- There are no unsafe responses during the start-up or shutdown phase. However, the disruption of blade weight balance leads to a slewing motion of the center shaft.
- Appendages that submerge in the water only when the rotor overspeed occurs can work as a passive braking system.
- The damping force caused by the submergence of PTO frame will contribute to the safety of the damaged case.

Author Contributions: Conceptualization, H.S., K.K., G.F., T.I., H.O. and H.A.; methodology, H.S., K.K. and H.A.; data curation, H.S. and K.K.; writing—original draft preparation, H.S.; writing—review and editing, H.S.; project administration, H.A. All authors have read and agreed to the published version of the manuscript.

Funding: This research was funded by the joint research among Electric Power Development Co., Ltd., Albatross Technology Inc., and Osaka University.

Data Availability Statement: Data are contained within the article.

Conflicts of Interest: Authors Gaku Fujita, Tomotake Imaoka, and Hiroyuki Ohira were employed by the company Electric Power Development Co., Ltd., Author Hiromichi Akimoto was employed by the company Albatross Technology Inc. The remaining authors declare that the research was conducted in the absence of any commercial or financial relationships that could be construed as a potential conflict of interest. The authors declare that this study received funding from Electric

Power Development Co., Ltd. The funder was not involved in the study design, collection, analysis, interpretation of data, the writing of this article or the decision to submit it for publication.

Nomenclature

λ	wavelength [m]
g	gravity acceleration [m/s^2]
H_w	wave height [m] (irregular wave case: significant wave height [m])
T_w	wave period [s] (irregular wave case: mean wave period [s])
θ_w	wave slope angle [rad]

Abbreviations

FOWTs	Floating offshore wind turbines
FAWT	Floating axis wind turbine
HAWT	Horizontal axis wind turbine
VAWT	Vertical axis wind turbine
TLP	Tension-leg platform
FVAWT	Floating vertical axis wind turbine
CFD	Computational fluid dynamics
LDV	Laser doppler velocity
PTO	Power take-off
DTU	Technical University of Denmark
BSG	Bulk specific gravity
NOWPHAS	Nationwide Ocean Wave information network for Ports and HARbourS
RAO	Response amplitude operator
ITTC	International Towing Tank Conference

References

1. Takata, T.; Takaoka, M.; Gonçalves, R.T.; Houtani, H.; Yoshimura, Y.; Hara, K.; Oh, S.; Dotta, R.; Malta, E.B.; Iijima, K.; et al. Dynamic Behavior of a Flexible Multi-Column FOWT in Regular Waves. *J. Mar. Sci. Eng.* **2021**, *9*, 124. [\[CrossRef\]](#)
2. Leroy, V.; Delacroix, S.; Merrien, A.; Bachynski-Polić, E.E.; Gilloteaux, J.-C. Experimental investigation of the hydro-elastic response of a spar-type floating offshore wind turbine. *Ocean Eng.* **2022**, *255*, 111430. [\[CrossRef\]](#)
3. Vittori, F.; Azcona, J.; Eguinoa, I.; Pires, O.; Rodríguez, A.; Morató, Á.; Garrido, C.; Desmond, C. Model tests of a 10MW semi-submersible floating wind turbine under waves and wind using hybrid method to integrate the rotor thrust and moments. *Wind Energy Sci.* **2022**, *7*, 5. [\[CrossRef\]](#)
4. Zhang, H.; Wen, B.; Tian, X.; Li, X.; Dong, Y.; Wang, M.; Peng, Z. Experimental study on mitigating vibration of floating offshore wind turbine using tuned mass damper. *Ocean Eng.* **2023**, *288*, 115974. [\[CrossRef\]](#)
5. Ghigo, A.; Faraggiana, E.; Giorgi, G.; Mattiazzo, G.; Bracco, G. Floating Vertical Axis Wind Turbines for offshore applications among potentialities and challenges: A review. *Renew. Sustain. Energy Rev.* **2024**, *193*, 114302. [\[CrossRef\]](#)
6. Paulsena, U.S.; Vita, L.; Madsenb, H.A.; Hattelc, J.; Ritchie, E.; Leban, K.M.; Berthlsen, P.A.; Carstensen, S. 1st DeepWind 5 MW baseline design. *Energy Procedia* **2012**, *24*, 27–35. [\[CrossRef\]](#)
7. Paulsena, U.S.; Madsenb, H.A.; Hattelc, J.H.; Baranc, I.; Nielsenb, P.H. Design Optimization of a 5 MW Floating Offshore Vertical-Axis Wind Turbine. *Energy Procedia* **2014**, *53*, 268–279. [\[CrossRef\]](#)
8. Borg, M.; Collu, M. A comparison on the dynamics of a floating vertical axis wind turbine on three different floating support structures. *Energy Procedia* **2013**, *35*, 22–32. [\[CrossRef\]](#)
9. Ishie, J.; Wang, K.; Ong, M.C. Structural Dynamic Analysis of Semi-Submersible Floating Vertical Axis Wind Turbines. *Energies* **2016**, *9*, 1047. [\[CrossRef\]](#)
10. Robertson, A.; Jonkman, J.; Masciola, M.; Song, H.; Goupee, A.; Coulling, A.; Luan, C. *Definition of the Semisubmersible Floating System for Phase II of OC4*; National Renewable Energy Laboratory: Golden, CO, USA, 2012.
11. Battisti, L.; Benini, E.; Brighenti, A.; Castelli, M.R.; Dell’Anna, S.; Dossena, V.; Persico, G.; Schmidt Paulsen, U.; Pedersen, T.F. Wind tunnel testing of the DeepWind demonstrator in design and tilted operating conditions. *Energy* **2016**, *111*, 484–497. [\[CrossRef\]](#)
12. Iwamatsu, S.; Suzuki, H.; Nihei, Y. Study on Elastic Response of Double-Rotor VAWTs. *J. Mar. Sci. Eng.* **2022**, *10*, 1400. [\[CrossRef\]](#)
13. Hand, B.; Cashman, A. Conceptual design of a large-scale floating offshore vertical axis wind turbine. *Energy Procedia* **2017**, *142*, 83–88. [\[CrossRef\]](#)
14. Yang, Y.; Guo, Z.; Zhang, Y.; Jinyama, H.; Li, Q. Numerical Investigation of the Tip Vortex of a Straight-Bladed Vertical Axis Wind Turbine with Double-Blades. *Energies* **2017**, *10*, 1721. [\[CrossRef\]](#)
15. Huijs, F.; Vlasveld, E.; Gormand, M.; Savenije, F.; Caboni, M.; LeBlanc, B.; Simao Ferreira, C.; Lindenburg, K.; Gueydon, S.; Otto, W.; et al. Integrated design of a semi-submersible floating vertical axis wind turbine (VAWT) with active blade pitch control. In Proceedings of the Journal of Physics: Conference Series, 1104, Trondheim, Norway, 17–19 January 2018.

16. Akimoto, H.; Tanaka, K.; Uzawa, K. Floating axis wind turbines for offshore power generation—a conceptual study. *Environ. Res. Lett.* **2011**, *6*, 044017. [[CrossRef](#)]
17. SeaTwirl. Available online: <https://seatwirl.com/> (accessed on 30 May 2024).
18. Hmedi, M.; Uzunoglu, E.; Zeng, C.; Gaspar, J.F.; Guedes Soares, C. Experimental Challenges and Modelling Approaches of Floating Wind Turbines. *J. Mar. Sci. Eng.* **2023**, *11*, 2048. [[CrossRef](#)]
19. Russo, V.; Contestabile, P.; Bardazzi, A.; Leone, E.; Iglesias, G.; Tomasicchio, G.R.; Vicinanza, D. Dynamic Loads and Response of a Spar Buoy Wind Turbine with Pitch-Controlled Rotating Blades: An Experimental Study. *Energies* **2021**, *14*, 3598. [[CrossRef](#)]
20. Takata, T.; Takaoka, M.; Houtani, H.; Hara, K.; Oh, S.; Malta, E.B.; Iijima, K.; Suzuki, H.; Gonçalves, R.T. Effect of Heave Plates on the Wave Motion of a Flexible Multicolumn FOWT. *Energies* **2022**, *15*, 7605. [[CrossRef](#)]
21. Robertson, A.; Wang, L. OC6 Phase Ib: Floating Wind Component Experiment for Difference-Frequency Hydrodynamic Load Validation. *Energies* **2021**, *14*, 6417. [[CrossRef](#)]
22. Tagliaferro, B.; Karimirad, M.; Altomare, C.; Goteman, M.; Martinez-Estevéz, I.; Capasso, S.; Dominguez, J.M.; Viccione, G.; Gomez-Gesteira, M.; Crespo, A.J.C. Numerical validations and investigation of a semi-submersible floating offshore wind turbine platform interacting with ocean waves using an SPH framework. *Appl. Ocean Res.* **2023**, *141*, 103757. [[CrossRef](#)]
23. Borg, M.; Pegalajar-Jurado, A.; Stiesdal, H.; Madsen, F.J.; Nielsen, T.R.L.; Mikkelsen, R.F.; Mirzaei, M.; Lomholt, A.K.; Bredmose, H. Dynamic response analysis of the TetraSpar floater in waves Experiment and numerical reproduction. *Mar. Struct.* **2024**, *94*, 103546. [[CrossRef](#)]
24. Bak, C.; Zahle, F.; Bitsche, R.; Kim, T.; Yde, A.; Henriksen, L.C.; Hansen, M.H.; Blasques, J.P.A.A.; Gaunaa, M.; Natarajan, A. *Description of the DTU 10MW Reference Wind Turbine*; DTU Wind Energy Report-I-0092; DTU Wind Energy: Kongens Lyngby, Denmark, 2013.
25. Akimoto, H.; Iijima, K.; Takata, Y. Feasibility study of the floating axis wind turbine preliminary model experiments. In Proceedings of the ASME 2017 36th International Conference on Ocean, Offshore and Arctic Engineering, Trondheim, Norway, 25–30 June 2017.
26. Real-Time NOWPHAS (The Nationwide Ocean Wave Information Network for Ports and HARbourS). Available online: <https://www.mlit.go.jp/kowan/nowphas/> (accessed on 30 May 2024).
27. Ishihara, T.; Liu, Y. Dynamic Response Analysis of a Semi-Submersible Floating Wind Turbine in Combined Wave and Current Conditions Using Advanced Hydrodynamic Models. *Energies* **2020**, *13*, 5820. [[CrossRef](#)]
28. Koo, B.J.; Goupe, A.J.; Kimball, R.W.; Lambrakos, K.F. Model tests for a floating wind turbine on three different floaters. *J. Offshore Mech. Arct. Eng.* **2014**, *136*, 020907. [[CrossRef](#)]
29. Ohta, M.; Komatsu, M.; Ito, H.; Kumamoto, H. Development of a V-shaped Semi-submersible Floating Structure for 7MW Offshore Wind Turbine. In Proceedings of the International Symposium on Marine and Offshore Renewable Energy, Tokyo, Japan, 28–30 October 2013.

Disclaimer/Publisher’s Note: The statements, opinions and data contained in all publications are solely those of the individual author(s) and contributor(s) and not of MDPI and/or the editor(s). MDPI and/or the editor(s) disclaim responsibility for any injury to people or property resulting from any ideas, methods, instructions or products referred to in the content.